Epidemic Spread of a Lesion-Forming Plant Pathogen – Analysis of a Mechanistic Model with Infinite Age Structure

James A. Powell*
Department of Mathematics and Statistics
Utah State University
Logan, Utah 84322-3900
USA

Ivan Slapničar
Faculty of Electrical Engineering, Mechanical
Engineering and Naval Architecture
University of Split
R. Boškovića b.b.
21000 Split
Croatia

Wopke van der Werf
Crop and Weed Ecology Group
Wageningen University
Bode 98, Postbus 430
6700 AK Wageningen
The Netherlands

September 8, 2004

Keywords: *Phytophthora*, integrodifference equations, Leslie matrices, fronts, invasion, rates of spread

AMS Subjects: 92D25, 92D99

Running Head: Spread of Lesion-Mediated Diseases

*Corresponding author, email: powell@math.usu.edu

Abstract

In many invasive species the number of invading individuals is proportional to the time since the population has established (its 'age'), not its density. Examples include plant diseases which spread via lesions, which grow on leaves with time and produce ever-increasing amounts of infective material. In this paper, a Leslie matrix model is developed to represent the age structure and reproductive potential due to lesions, particularly for mycelial colonies associated with fungal plant pathogens. Lesion size (and therefore age) is bounded by leaf size, which can be quite large, leading to large matrices. The production of new mycelial colonies is affected by dispersal of spores from the reproductive age-classes of existing colonies, so that dispersal must be included in the matrix model by convolution operators. The infinite-dimensional version of the model is more tractable than the large, finite models, and is used to determine an upper bound on rates of invasion. The model is applied to model the life history of the oömycete *Phytophthora infestans*, causal agent of potato late blight disease. It is shown that the infinite-dimensional model closely predicts behavior of finite dimensional models, cut off at certain age-classes of lesions because of finite leaf size. Surprisingly, the infinite-dimensional model is more tractable than finite-dimensional model versions, yielding robust results for practical situations.

1 Introduction

The spread of disease or invasive species has been the subject of mathematical, biological, and epidemiological interest since the turn of the nineteenth century. The progress of 'waves of invasion' affect humans directly, and consequently predicting the rate at which invasions and epidemics move has been an issue of applied interest in mathematics since Fisher [7], Kolmogorov [14] and Skellam [30]. Modern treatments have been extended to systems of competing species (see, for example, the companion papers [40] and [20] of the team Weinberger, Lewis and Li) and populations with significant age structure (e.g. (Neubert & Caswell, [19]). Classically, the spread of an invasion or epidemic has been related to the density of dispersing units (spores, seeds, juveniles seeking new territories), which is generally proportional to the density of the established population, and the mean dispersal distance of these propagules. Since the density of an established population is generally limited, the density of propagules has an upper bound and it is reasonable to expect that propagation speeds should also be asymptotically limited.

However, as pointed out by Shigesada and Kawasaki [29], many populations have the property that the number of invading propagules grows with the age (spatial extent of the basic infected unit or patch, as opposed to the density) of the established population. Examples include fungal pathogens, Gypsy moth (*Lymantria dispar*), cheat grass (*Bromus tectorum*) in the American West,

and native-invasive species like Southern and Mountain Pine Beetles (*Dendroctonus frontalis* and *pondersosae*, respectively). In all of these cases, the basic small-scale unit of infection is a spot or lesion. For either lesions on a leaf (as in *Botrytis elliptica*, responsible for fire disease in lilies, or *Phytophthera infestans*, potato late blight) or an infectious spot of trees (as in Southern Pine Beetle *Dendroctonus frontalis*), the number of propagules available to start new infestations is related to the age of the lesion or spot, not its density. As pointed out by Shigesada and Kawasaki, this can result in continually accelerating invasions.

Plant diseases, caused by fungi, bacteria, viruses and other microorganisms, are a leading cause of agricultural crop loss and are therefore of particular interest. One of the most important plant diseases in the world in terms of damage and control costs is late blight disease in potatoes and tomatoes, caused by the oömycete *Phytophthora infestans* [11]. Oömycetes are a distinct group of plant pathogens which until recently were regarded as fungi, but have now been classified as a distinct taxon, more related to algae than to fungi. Epidemiologically however, with regard to the spread of disease in plant populations, oömycetes have much in common with fungal pathogens. Their life cycle includes the same steps of infection, formation of biomass ('mycelium') in the host, spatial expansion of the affected area ('lesion'), and formation and dispersal of propagules ('spores'). For purposes of this paper, we will therefore speak about fungi when we discuss relevant epidemiological processes. The oömycete *P. infestans* is taken as an example organism because of its practical importance and because its life cycle attributes are well studied.

Reproductive strategies of fungi are varied in the extreme. A common theme for plant pathogenic fungi is production of spores that are spread through the air. Spores are released, spread with wind and/or rain, and after landing on (nearby) plant surfaces they potentially cause new lesions. Once a lesion is initiated, the pathogenic fungus colonizes the surrounding plant tissue by sending out hyphae and extracting nutrients from this tissue. The lesion grows at a relatively constant radial rate. Several days after a region of tissue has been colonized by hyphae, sporulating bodies develop from the local mycelium and spores can be produced and released for some time. After this period, the local mycelium dies and sporulation stops. In the mean time the colonized area, and therefore the lesion, has expanded.

For *P. infestans* this general pattern of latency, infectiousness and senescence results in circular lesions with an infective annulus some distance behind the (invisible) leading edge of the lesion and

dead tissue some radial distance behind that. One may think of lesions as the basic infection unit of *P. infestans* (Zadoks and Schein [41]). Release and spread of spores from an annular sporulating region inside each lesion, followed by infection, is the basic mode of propagation of *P. infestans* through a crop.

The mathematical analysis of plant disease epidemics in particular is a matter of great practical relevance, and substantial effort has therefore been invested in generating predictions of spatial spread of plant disease (van den Bosch et al., [33, 34, 35, 36] and linking theories of epidemics of plant diseases to those of animals and humans (e.g. Segarra et al., [28]; Diekmann & Heesterbeek, [4]). Almost exclusively, theories of plant disease epidemics have been based on the analysis of ordinary and partial differential equations and integral equations. Such approaches require that the life history of individuals (often lesions of the disease on the host), e.g. their fecundity versus age, be quantified at the individual lesion level. Such an approach seems awkward in the case of mycelial colonies for which the reproductive potential is limited only by the amount of resource space that is available for colonization, and not by any intrinsic characteristic of the individual. Recent progress (Neubert & Caswell, [19]; Caswell et al., [2]) in the analysis of matrix models (for population growth) in combination with integrodifference equations (for dispersal) allow us to develop a model in which this unbounded reproductive potential of the individual is made explicit. In order to make the model intuitively appealing, it is developed for the pathogen *Phytophthora infestans*. It should be kept in mind, however, that the proposed methodology are applicable to any organism organized in radially expanding colonies, and whose reproductive potential increases with age as the colonized area and annulus of reproductively active material increases. Thus, this model may find application for microscopic as well as macroscopic fungi (e.g. Lamour, [17]), pathogenic organisms that infecting a living hosts, decomposers (”saprophytes”) that colonize soil or detritus, as well as bark beetles, cheat grass, and the like.

Below we will propose a discrete-time, continuous-space model for the density of lesions. We will view a lesion, or spot, as the basic infectious unit, and examine how an epidemic progresses when the number of propagules produced by a lesion grows linearly with the age of the lesion (as in most fungal pathogens). Below we will propose a discrete-time, continuous-space model for the density of lesions in an uninfected substrate. Our objectives will be to:

- show how the demographics of lesions of - for instance - plant disease causing organisms

can be captured in a Leslie matrix formalism,

- derive the asymptotic propagation properties of such an infinite dimensional matrix model when combined with integrodifference equations to represent dispersal,
- show that the infinite dimensional version is more tractable than the finite dimensional age structure, and
- demonstrate that the asymptotic infinite dimensional results provide a reasonable, close upper bound on propagation speeds.

We will derive and analyze the model specifically in the case of potato late blight, but the results should be generally applicable to diseases and invasions where infectiousness increases continually with the age of the basic infective unit, a lesion.

2 Modeling the Population Dynamics of Fungal Invaders

2.1 Age Structure of Lesions – Dynamics on a Leaf

An individual lesion on a leaf grows at a measurable and well-defined radial growth rate, Δr, per day, and after a certain latency period ($LP =$ five days for *P. infestans*) the invaded area of the leaf sporulates for a certain number of days ($IP = 1$ day). The progress of an individual late blight lesion on a single leaf is depicted in Figure 1. During the infectious period spores are released at a given rate, SI, per unit area per day, and these spores disperse. Some fraction of spores which settle from the air are intercepted by leaves (with probability P_{int}), and of these intercepted spores a fraction, P_{inf}, successfully germinates and infects the plant (provided it does not land on area already occupied by a lesion). The parameters of the model and nominal values are listed in Table 1.

When a lesion is t days old, the area that it adds is the difference between the area it is, $A_t = \pi(t\Delta r)^2$ and the area it will become on the next day, $A_{t+1} = \pi(t+1)^2\Delta r^2$. Thus,

$$\Delta A_{t+1} = A_{t+1} - A_t = \pi\Delta r^2\left[(t+1)^2 - t^2\right] = (2t+1)\pi\Delta r^2 \approx 2\pi t\Delta r^2.$$

Consequently, when a lesion is $LP+1$ or more days old, the area which is sporulating is the area which was added to the lesion LP days ago. Since N_t^n is the density of lesions of age t days on

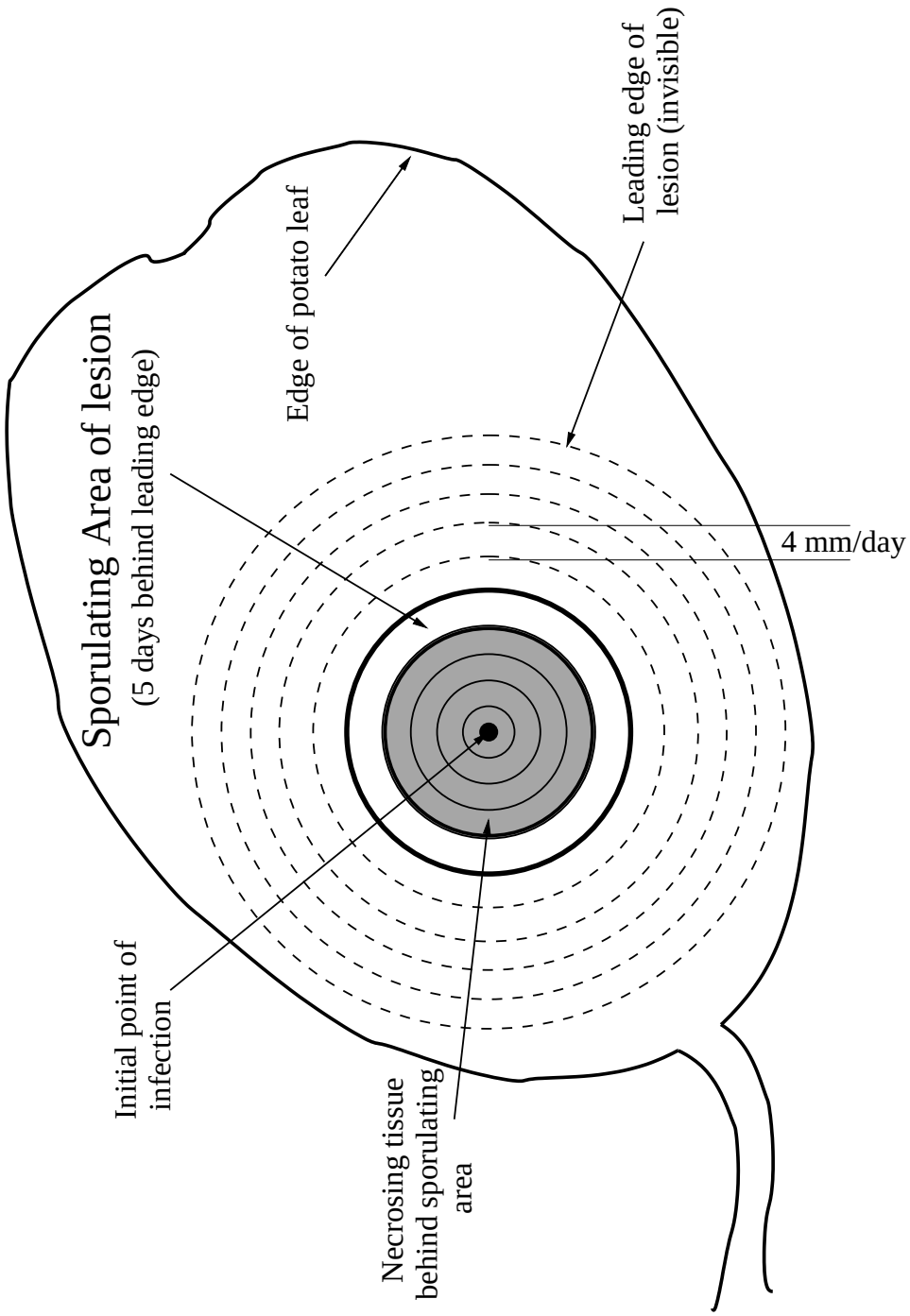

Figure 1: Diagram of progress of a single lesion through a leaf. The actual furthest location of the lesion, denoted as the dashed circle, is invisible. The edge of the sporulating area, indicated above as the area between heavy solid circles, emerges from the leaf surface LP days after infection and produces sporulating bodies. In the radial region behind the sporulating area the lesion has used up available resources. A typical daily growth rate for a late blight lesion is 4 millimeters per day, with a latency period of $LP = 5$ days.

Parameter	Description	Nominal Value (Units)
SI	Sporulation Intensity	10^8 (Spores/meter^2/day)
LP	Latency Period	5 (days)
IP	Infectious Period	1 (day)
P_{inf}	Probability of infection per landed spore	10^{-2}
P_{int}	Probability of interception per dispersed spore	10^{-1}
Δr	Radial growth rate of lesions	4×10^{-3} (meter/day)
LAI	Leaf Area Index	5 (meter^2 crop/meter^2 soil)
σ	Mean dispersal distance from parent lesion	1 (meter)

Variable	Description	(Units)
t	Age of Lesion	(days)
n	Day of Simulation (independent variable)	(days)
N_t^n	Density of Lesions of age t on day n	(number/meter^2)
A_t	Area of a lesion of age t days	(meter^2)
ΔA_t	Newly grown area for a t-day-old lesion	(meter^2)

Table 1: Parameters and variables of the *Phytophthora infestans* population model. Nominal values are gleaned from [8] and [26]as well as estimates provided by field researchers [32], using the rule of thumb that each parent lesion produces about ten daughter lesions in ideal circumstances.

day n, the density of spores produced by these lesions is

$$\text{SP}_t^n = N_t^n \times SI \times \Delta A_{t-LP} \approx N_t^n \times SI \times 2\pi\Delta r^2(t - LP), \quad (t > LP).$$

This is an idealization based on the assumption that leaves of the plant are much larger than the lesions; stability of our results to relaxation of this assumption will be investigated in later sections. The density of spores produced on day n is thus is given by

$$\text{SP}^n = SI \times \underbrace{\sum_{t=LP+1}^{n} N_t^n \Delta A_{t-LP}}_{\text{Area of Infectious Lesions}} \approx SI \times 2\pi\Delta r^2 \sum_{t=LP+1}^{n} N_t^n (t - LP).$$

Assuming that all dispersal happens locally, the density of spores arriving is the density of spores produced on the previous day, SP^n,

and a model for reproduction of lesions can be written

$$\begin{aligned} N_1^{n+1} &= P_{\text{int}} \times P_{\text{inf}} \times P_{\text{un}}(N_1^n, N_2^n, \cdots) \times \text{SP}^n \\ N_2^{n+1} &= N_1^n \\ &\vdots \end{aligned}$$

$$
\begin{aligned}
N_t^{n+1} &= N_{t-1}^n \\
&\vdots
\end{aligned}
$$

The combination of probabilities in the first line is the probability of the composite event that (first) a spore lands on a leaf and is not subsequently knocked off (P_{int}), that (second) the spore is able to germinate, penetrate the outer skin of the leaf and establish in the host(P_{inf}), and finally that (third) the spore has landed on leaf area not currently occupied by a lesion (P_{un}). Probabilistic parameters for potato late blight are set using the 'rule of thumb' that 1 parent lesion produces a net 10 daughter lesions in the Netherlands in ideal circumstances [32]. The probability of a spore landing on unoccupied leaf area can be calculated from the ratio of the total leaf area and the total area unoccupied by lesions,

$$
\begin{aligned}
P_{\text{un}}(N_1^n, N_2^n, \cdots) &= \max\left[\frac{LAI - \sum_{t=LP+1}^{n} N_t^n \Delta A_{t-LP}}{LAI}, 0\right] \\
&\approx \max\left[1 - \frac{2\pi\Delta r^2}{LAI} \sum_{t=LP+1}^{n} N_t^n\ (t - LP), 0\right]. \qquad (1)
\end{aligned}
$$

2.2 The Effects of Dispersal – Spread Between Leaves

To investigate the spread of lesions one must describe how spores produced in one location arrive at a different location. Dispersal can occur by wind, by raindrops 'splattering' [22], or even ballistically by pressurized expulsion from sporangia; models can range from relatively simple probabilistic descriptions to solution of turbulent diffusion equations in and above the crop [12]. We will a probabilistic approach and introduce a dispersal kernel, $K(x)$, the probability of spores produced at $x = 0$ dispersing to the location x. The density of spores, $S(x)$, arriving at a location x, given a spatial distribution of spore production, $P(x)$, is

$$
S(x) = \int_{-\infty}^{\infty} K(x - y)P(y)\, dy \stackrel{\text{def}}{=} K * P.
$$

One may think of this as summing the probabilities that spores produced at location y, numbering $P(y)\, dy$, will disperse the distance $(x - y)$ to the location x. Integrating defines the convolution, $S = K * P$.

To include dispersal in the age-structured model we interpret N_t^n as the spatial density of lesions which are t days old on day n. The number of spores arriving at a given spatial location is

then

$$\text{S\_arr} = SI \times \sum_{t=LP+1}^{\infty} (K * N_t^n)\Delta A_{t-LP} \approx SI \times 2\pi\Delta r^2 \sum_{t=LP+1}^{\infty} (t-LP)K * N_t^n.$$

Writing $\vec{V}_n = (N_1^n, N_2^n, \cdots N_t^n, \cdots)^T$, the spatio-temporal dynamics are governed by a nonlinear Leslie matrix with dispersal operations:

$$\vec{V}_{n+1} = (\mathbf{B} \circ \mathbf{K}) * \vec{V}_n, \tag{2}$$

where $\mathbf{B}$ is the infinite dimensional matrix

$$\mathbf{B} = \begin{pmatrix} 0 & 0 & 0 & 0 & 0 & RP_{\text{un}} & 2RP_{\text{un}} & 3RP_{\text{un}} & \cdots & (t-LP)RP_{\text{un}} & \cdots \\ 1 & 0 & 0 & 0 & 0 & 0 & 0 & 0 & 0 & 0 & \cdots \\ 0 & 1 & 0 & 0 & 0 & 0 & 0 & 0 & 0 & 0 & \cdots \\ 0 & 0 & 1 & 0 & 0 & 0 & 0 & 0 & 0 & 0 & \cdots \\ 0 & 0 & 0 & 1 & 0 & 0 & 0 & 0 & 0 & 0 & \cdots \\ 0 & 0 & 0 & 0 & 1 & 0 & 0 & 0 & 0 & 0 & \cdots \\ \vdots & \vdots & \vdots & \vdots & \vdots & \ddots & \vdots & \vdots & \vdots & \vdots & \ddots \end{pmatrix}, \tag{3}$$

K is the matrix composed of dispersal kernels,

$$\mathbf{K} = \begin{pmatrix} 0 & 0 & 0 & 0 & 0 & K(x) & K(x) & K(x) & \cdots & K(x) & \cdots \\ \delta(x) & 0 & 0 & 0 & 0 & 0 & 0 & 0 & 0 & 0 & \cdots \\ 0 & \delta(x) & 0 & 0 & 0 & 0 & 0 & 0 & 0 & 0 & \cdots \\ 0 & 0 & \delta(x) & 0 & 0 & 0 & 0 & 0 & 0 & 0 & \cdots \\ 0 & 0 & 0 & \delta(x) & 0 & 0 & 0 & 0 & 0 & 0 & \cdots \\ 0 & 0 & 0 & 0 & \delta(x) & 0 & 0 & 0 & 0 & 0 & \cdots \\ \vdots & \vdots & \vdots & \vdots & \vdots & \ddots & \vdots & \vdots & \vdots & \vdots & \ddots \end{pmatrix}, \tag{4}$$

and the operation of element-by-element multiplication (Hadamard product) is denoted by '$\circ$'. The composite constant,

$$R = 2\pi P_{\text{int}} P_{\text{inf}}\, SI\, \Delta r^2, \tag{5}$$

is the net number of new lesions produced in an unoccupied environment by an $LP+1$-day old lesion (the youngest lesion which is infectious). Nonlinearity is introduced into the system by P_{un}, computed on a daily basis for each location.

3 An Upper Bound for the Speed of Invasion

3.1 Review of the Minimum Wave Speed Calculation

We summarize here (and adopt the notation of) arguments presented by Neubert and Caswell [19] for finite Leslie matrices with dispersal, which are in turn based on results of Weinberger [38, 39],

Kot et al. [15, 16] and Neubert et al. [21]. Estimating the speed of the wave of invasion, or front, requires analyzing the linearization of (2). For sufficiently small N_t^n (for example, in advance of the main infestation), $P_{\text{un}} \approx 1$ and the dynamics can be written

$$\vec{V}_{n+1} = (\mathbf{A} \circ \mathbf{K}) * \vec{V}_n, \tag{6}$$

where $\mathbf{A}$ is the linearization of $\mathbf{B}$,

$$\mathbf{A} = \lim_{P_{\text{un}} \to 1} \mathbf{B}.$$

Sufficiently far in advance of the front, the spatial shape of solutions may be approximated

$$\vec{V}_n \sim e^{-sx}\vec{w},$$

where $\vec{w}$ is a vector describing relative abundances in different age-classes of lesions, each dropping off exponentially at a rate, s, in the direction, x, in advance of the front. For a front traveling at a distance v per iteration, then

$$\vec{V}_{n+1}(x) = \vec{V}_n(x - v) \sim e^{sv-sx}\vec{w},$$

and substituting into (6),

$$e^{sv-sx}\vec{w} = \left[(\mathbf{A} \circ \mathbf{K}) * e^{-sx}\right] \vec{w} = e^{-sx} \left[\mathbf{A} \circ \mathbf{M}(s)\right] \vec{w}. \tag{7}$$

Here $\mathbf{M}(s)$ is the moment-generating matrix computed element-by-element,

$$\mathbf{M}(s) = \int_{-\infty}^{\infty} e^{sy}\mathbf{K}(y)\, dy. \tag{8}$$

To see why, consider one of the nonzero elements of $\mathbf{K}$ in the first row:

$$K * e^{-sx} = \int_{-\infty}^{\infty} e^{-s(x-y)}K(y)\, dy = e^{-sx} \int_{-\infty}^{\infty} e^{sy}K(y)\, dy = e^{-sx}M(s),$$

where $M(s)$ is the (scalar) moment generating function for the dispersal kernel K.

Cancelling common factors in (7) gives an eigenvalue problem

$$e^{sv}\ \vec{w} = \left[\mathbf{A} \circ \mathbf{M}(s)\right] \vec{w} \stackrel{\text{def}}{=} \mathbf{H}(s)\ \vec{w}. \tag{9}$$

Suppose $\mathbf{H}(\mathbf{s})$ has (countable) eigenvalues $\lambda_1(s), \lambda_2(s), \cdots$, non-increasingly ordered by magnitude. The *minimum wave speed conjecture* is that the speed of the wave of invasion is smaller than v^*, where

$$v^* = \min_{0<s<\hat{s}} \left[\frac{1}{s} \ln\left(\lambda_1(s)\right)\right], \tag{10}$$

where $\hat{s}$ is the maximum s for which all elements of $\mathbf{M}(s)$ are defined.

For waves of invasion starting from compact initial conditions, the speed of advance should be slower than v^*, an argument elegantly stated recently by Neubert and Caswell [19]. In many, but not all, cases it can also be shown that fronts accelerate to the minimum speed, in which case it becomes the asymptotic speed of fronts. Taking a dynamic perspective suggests that the 'minimum' speed should be the asymptotic front speed. This perspective harks back to Kolmogorov et. al. [14], but was stated in the context of dynamics by Dee and Langer [3] and Powell et. al. [23, 24]. In a traveling frame of reference, $z = x - nv$, the solution to the linearized equation can be written

$$\vec{V}_n = \mathcal{FT}^{-1}\left[e^{-invk}\mathbf{H}(ik)\hat{\vec{V}}_0\right], \tag{11}$$

where $\mathcal{FT}^{-1}$ denotes the inverse Fourier transform, $\hat{\vec{V}}_0$ is the Fourier transform of the initial data and **H** is as in the discussion above, but evaluated with the substitution $s \to ik$. Asymptotically, using the power method, the integrand in (11) can be written

$$e^{-invk}\mathbf{H}(ik)\hat{\vec{V}}_0 = a_1 e^{-invk}\lambda_1^n(ik)\hat{\vec{e}}_1(k) + \cdots = a_1 \exp\left[n\left\{\ln\left(\lambda_1(ik)\right) - ivk\right\}\right]\hat{\vec{e}}_1(k) + \cdots,$$

where λ_1 is the largest magnitude eigenvalue and $\hat{\vec{e}}_1$ the associated eigenvector. Thus

$$\vec{V}_n \approx \frac{1}{2\pi}\int_{-\infty}^{\infty} e^{ikz}\exp\left[n\left\{\ln\left(\lambda_1(ik)\right) - ivk\right\}\right]\hat{\vec{e}}_1(k)\, dk. \tag{12}$$

The integral in (12) can be evaluated using steepest descents to get a further asymptotic approximation. The stationary point satisfies

$$\frac{d}{dk}\left[\ln\left(\lambda_1(ik)\right) - ivk\right] \stackrel{\text{set}}{=} 0. \tag{13}$$

If k^* is the stationary point solving (13), an associated speed for the traveling frame of reference, v^*, is chosen so that the wave neither grows nor shrinks in this frame of reference, that is

$$\text{Real}\ \left[\ln\left(\lambda_1(ik^*)\right) - iv^*k^*\right] = 0. \tag{14}$$

Working through the algebra, one finds that the solutions to (13, 14) correspond exactly to (10), using the substitution $ik^* \to s^*$.

The dynamic interpretation leads to a useful convergence estimate. The quantity maximized in (13) is the exponential growth rate of of waves traveling with speed v. The stationary point, k^*, has

maximal growth rate; the method of steepest descents is a statement that asymptotic front solutions grow from the most unstable Fourier mode in an ensemble describing the initial data. The choice of v^* via (14) determines the speed of the most unstable mode using a stationary phase argument. This suggests that the minimal wave speed, v^*, should not only be an upper bound, but also the asymptotic speed observed, since it results from the growth and propagation of the most unstable wave component of the solution. Moreover, an asymptotic form for the solution is predicted,

$$\vec{V}_n(z) \sim e^{ik^*z}\,\frac{a_1(k^*)}{\sqrt{2n\pi}}\exp\left[\ln\left(\lambda_1(ik^*)\right) - iv^*k^*\right]\left[\frac{\lambda_1''(ik^*)}{\lambda_1(ik^*)} - \left(\frac{\lambda_1'(ik^*)}{\lambda_1(ik^*)}\right)^2\right]^{-\frac{1}{2}}\hat{\vec{e}}_1(k^*) + c.c. \quad (15)$$

Incorporating the factor of $\sqrt{n}$ from the denominator of (15) into the exponent indicates that front speeds should converge from below to the asymptotic speed,

$$v_{\text{observed}} = v^*\left(1 - \frac{\ln(n)}{2nk^*}\right), \quad (16)$$

which will be used below.

3.2 Determination of Maximum Eigenvalue

Calculation of v^* is on firm ground when the matrices involved are finite. For our system, however, the matrices concerned are infinite dimensional and calculating the maximum eigenvalue of $\mathbf{H}(s)$ is not straightforward. Recalling that we have taken $M(s)$ to be the (scalar) moment generating function for the dispersal kernel $K(x)$, and specifying $LP = 5$, we can write

$$\mathbf{H}(s) = \begin{pmatrix} 0 & 0 & 0 & 0 & 0 & R\,M(s) & 2R\,M(s) & 3R\,M(s) & \cdots & (t-5)R\,M(s) & \cdots \\ 1 & 0 & 0 & 0 & 0 & 0 & 0 & 0 & 0 & 0 & \cdots \\ 0 & 1 & 0 & 0 & 0 & 0 & 0 & 0 & 0 & 0 & \cdots \\ 0 & 0 & 1 & 0 & 0 & 0 & 0 & 0 & 0 & 0 & \cdots \\ 0 & 0 & 0 & 1 & 0 & 0 & 0 & 0 & 0 & 0 & \cdots \\ 0 & 0 & 0 & 0 & 1 & 0 & 0 & 0 & 0 & 0 & \cdots \\ \vdots & \vdots & \vdots & \vdots & \vdots & \ddots & \vdots & \vdots & \vdots & \vdots & \ddots \end{pmatrix}, \quad (17)$$

where R is defined by (5).

To analyze the spectrum of $\mathbf{H}(s)$, we consider the linear operator $\mathbf{H} : l^1 \to l^1$ defined by

$$(x_1, x_2, x_3, \cdots) \to \left(\rho\sum_{k=6}^{\infty}(k-5)x_k, x_1, x_2, x_3, \cdots\right), \qquad \rho \stackrel{\text{def}}{=} R\,M(s), \quad (18)$$

where l^1 is the Banach space of all real sequences $\mathbf{x} \stackrel{\text{def}}{=} (x_1, x_2, x_3, \cdots)$ such that $\sum |x_k| < \infty$. The matrix $\mathbf{H}(s)$ is the representation of $\mathbf{H}$ in the standard basis $\mathbf{e}_k \stackrel{\text{def}}{=} \delta_{ik}$, where δ_{ik} is the Kronecker

symbol. The space l^1 is natural, since the total number of lesions and spores is always finite. The domain of **H** is

$$\text{Dom } \mathbf{H} = \left\{ \mathbf{x} \in l^1 : \left| \sum_{k=6}^{\infty} (k-5) x_k \right| < \infty \right\},$$

reflecting the previous natural assumption, since the summation in is proportional to the total number of spores produced (large, but finite).

For each λ, the operator $\mathbf{H}_\lambda \stackrel{\text{def}}{=} \mathbf{H} - \lambda \mathbf{I}$ is defined by

$$(x_1,\ x_2,\ x_3,\ \cdots) \to \left(-\lambda x_1 + \rho \sum_{k=6}^{\infty} (k-5) x_k,\ x_1 - \lambda x_2,\ x_2 - \lambda x_3,\ x_3 - \lambda x_4,\ \cdots \right). \quad (19)$$

Our aim is to find all eigenvalues of **H**, that is, the set of all $\lambda \in \mathbb{C}$ which satisfy $\mathbf{H}_\lambda \mathbf{x} = 0$, $\mathbf{x} \neq 0$. The set of all eigenvalues is called the point spectrum of **H** [31, Section V.4] and is denoted by $\sigma_p(\mathbf{H})$. For each eigenvalue λ, any $\mathbf{x} \in \text{Dom } \mathbf{H}$ such that $\mathbf{H}_\lambda \mathbf{x} = 0$ is a corresponding eigenvector. Equating the right hand side of (19) to zero gives

$$x_k = \lambda x_{k+1}, \quad k = 1, 2, 3, \cdots. \quad (20)$$

For the first component, using (20) and induction, we have

$$-\lambda x_1 + \rho \sum_{k=6}^{\infty} (k-5) \frac{x_1}{\lambda^{k-1}} = 0. \quad (21)$$

¿From (20) it follows that any non-trivial solution of $\mathbf{H}_\lambda \mathbf{x} = 0$ must satisfy $x_1 \neq 0$, so (21) implies

$$-\lambda + \rho \sum_{k=6}^{\infty} (k-5) \frac{1}{\lambda^{k-1}} = -\lambda + \rho \frac{1}{\lambda^3} \sum_{k=1}^{\infty} \frac{k}{\lambda^{k+1}} = 0.$$

We seek the largest eigenvalue and expect the population of lesions to grow, so we confine ourselves to the case $|\lambda| > 1$. Using differentiation of geometric series, we have

$$-\lambda + \rho \frac{1}{\lambda^3} \frac{1}{(\lambda - 1)^2} = 0.$$

Therefore, eigenvalues of **H** are zeros of the polynomial

$$\lambda^6 - 2\lambda^5 + \lambda^4 - \rho = 0, \quad (22)$$

which also satisfy $|\lambda| > 1$. From (20) we see that the corresponding eigenvectors are

$$\mathbf{x} = \left(1, \frac{1}{\lambda}, \frac{1}{\lambda^2}, \frac{1}{\lambda^3}, \cdots \right).$$

Obviously, $\mathbf{x} \in l^1$, and since $|\lambda| > 1$ implies $\sum(k-5)/|\lambda^k| < \infty$, we also have $\mathbf{x} \in \text{Dom}\,\mathbf{H}$. Interestingly, the roots of (22) can be computed exactly in terms of radicals (e.g. by *Mathematica*), and they all lie outside the unit circle. Inspecting all six roots, we see that the largest magnitude root of the polynomial (22) is

$$\lambda_1(s) = \frac{1}{3} + \frac{2^{1/3}}{3\left(2+27\sqrt{\rho}+\sqrt{108\sqrt{\rho}+729\rho}\right)^{1/3}} + \frac{\left(2+27\sqrt{\rho}+\sqrt{108\sqrt{\rho}+729\rho}\right)^{1/3}}{3\cdot 2^{1/3}}. \quad (23)$$

Since in deriving this expression we have assumed that $|\lambda| > 1$ and $\lambda_1(s) > 1$ for $\rho \neq 0$, we conclude that (23) gives the largest eigenvalue of the operator $\mathbf{H}(s)$ from (17). By analysis similar to one in [9, Section 3] (see also [31, Section V.4, Problem 11]), we can show that the residual spectrum of $\mathbf{H}$ is the set $\sigma_r(\mathbf{H}) = \{\lambda \in \mathbb{C} : |\lambda| \leq 1,\ \lambda \neq 1\}$ and the continuous spectrum of $\mathbf{H}$, $\sigma_c(\mathbf{H})$, contains only the point $\lambda = 1$. The derivation of these results is beyond the scope of this paper and is omitted, since they do not correspond to invading lesion populations.

Since $\rho = RM(s)$, expression (23), together with (10), allows for prediction of rates of invasion as a function of parameters describing the fecundity, dispersal, and infectiousness of the disease. This formula is useful, in that the maximum eigenvalue and therefore asymptotic speed of invasion for any lesion-based pathogen can be determined without setting up arbitrarily large population matrices and extracting eigenvalues numerically. In addition, since the maximum eigenvalue $\lambda_1(s)$ behaves like $O(\rho^{1/6})$ from (23), the formula also allows us to conclude that the predicted upper bound v^* from (10) is stable for very infectious diseases ($R \gg 1$) in the sense that small changes of the parameters from Table 1 or entries in the matrix cause only proportionally small changes in v^*.

3.3 Finite Dimensional Case

In general one may expect speeds of the nonlinear invasion, governed by the infinite system (2), to approach speeds predicted for the linear system, (6), using the minimum-speed methodology. An new wrinkle occurs because of age structure: invasions are initialized with lesions of age 1, and the progress of disease is modeled by application of *finite* operators, whose number of entries grows by one daily. Consequently there are two convergence issues to keep in mind. The first concerns the rate at which nonlinear fronts of fixed dimensionality approach the minimal wave speed. The second, novel issue concerns the rate at which the finite dimensional eigenvalues,

presumably controlling the speed of propagation in the age-structured population, approaches the largest eigenvalue in the infinite system.

Let $\mathbf{H}_m(s)$ be the leading $m \times m$ submatrix of $\mathbf{H}(s)$ from (17), where ρ is defined by (18). Let $\lambda_1^{(m)}(s)$ denote the largest positive eigenvalue of $\mathbf{H}_m(s)$. To estimate the effect of reduction to finite dimension for the linearized case, we need to compute $\lambda_1^{(m)}(s)$, and compare it to $\lambda_1(s)$. First, since $\mathbf{H}_m(s)$ is non-negative and irreducible, by the Perron-Frobenius Theorem [18, Theorem 9.2.1] it follows that the absolutely largest eigenvalue of $\mathbf{H}_m(s)$ is real and positive. Thus $\lambda_1^{(m)}(s)$ exists for every m and is equal to the spectral radius of $\mathbf{H}_m(s)$. Figure 2 shows the eigenvalues of $\mathbf{H}_{100}(s)$ for $\rho = 10$; we see six distinct eigenvalues (there are five distinct eigenvalues for odd m), and the rest of the eigenvalues are close to the outer border of the unit circle.

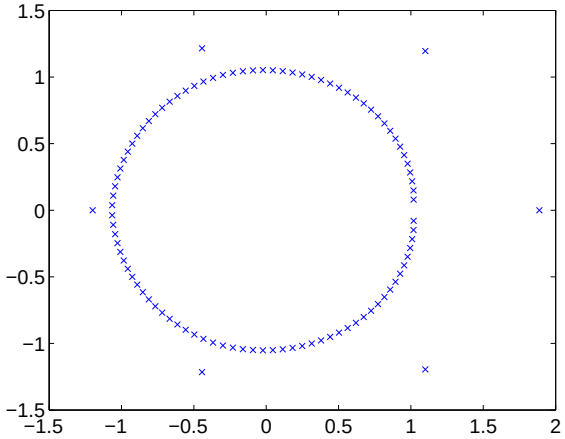

Figure 2: Eigenvalues of $\mathbf{H}_{100}(s)$ for $\rho = 10$. Note the six eigenvalues outside the unit circle, converging to the six roots of the polynomial $\lambda^6 - 2\lambda^5 + \lambda^4 - \rho = 0$ in the infinite case.

Let us prove that the sequence of largest eigenvalues, $\{\lambda_1^{(m)}(s)\}$, is convergent for ρ fixed. We do this by showing that the sequence is bounded and increasing. Let

$$D_m = \operatorname{diag}\left(1, 1, 1, 1, 1, \frac{1}{\rho}, \frac{1}{2\,\rho}, \frac{1}{3\,\rho}, \cdots, \frac{1}{(n-5)\,\rho}\right),$$

and set

$$\mathbf{H}_m^{\dagger}(s) = D_m^{-1}\mathbf{H}_m D_m.$$

The first row of $\mathbf{H}_m^{\dagger}(s)$ is

$$(0, 0, 0, 0, 0, 1, 1, 1, \cdots, 1),$$

the first sub-diagonal is

$$\left(1, 1, 1, 1, \rho, 2, \frac{3}{2}, \frac{4}{3}, \frac{5}{4}, \cdots, \frac{m-5}{m-4}\right),$$

and the remaining elements of $\mathbf{H}_m^\dagger(s)$ are zero. By applying Geršgorin's Theorem [18, Theorem 7.2.1] columnwise, it follows that all eigenvalues are included in the union of discs which are centered at zero and have radii

$$r_1 = r_2 = r_3 = r_4 = 1, \quad r_5 = \rho, \quad r_k = \frac{k}{k-1} + 1, \quad k = 2, 3, \cdots, m-5.$$

Therefore,

$$|\lambda_i(\mathbf{H}_m^\dagger(s))| \leq \max\{\rho, 3\}, \quad i = 1, 2, \cdots m.$$

Since the matrices $\mathbf{H}_m^\dagger(s)$ and $\mathbf{H}_m(s)$ have identical eigenvalues the sequence $\{\lambda_1^{(m)}(s)\}$ is bounded. Further, let $P_m(\lambda, s)$ be the characteristic polynomial of $\mathbf{H}_m(s)$. Since $\mathbf{H}_m(s)$ has the form of the companion matrix, it is easy to see that

$$P_m(\lambda, s) = \lambda^m - \rho\lambda^{m-6} - 2\,\rho\,\lambda^{m-7} - 3\,\rho\,\lambda^{m-8} - \cdots - (m-6)\,\lambda - (m-5).$$

By induction we have

$$P_{m+1}(\lambda, s) = \lambda\, P_m(\lambda, s) - (m-4).$$

Since $P_m(\lambda_1^{(m)}(s), s) = 0$, we have

$$P_{m+1}\left(\lambda_1^{(m)}(s), s\right) = \lambda_1^{(m)}(s) \cdot 0 - (m-4) < 0.$$

Therefore, $P_{m+1}(\lambda, s)$ has a real zero which is greater than $\lambda_1^{(m)}(s)$. It follows that the sequence $\{\lambda_1^{(m)}(s)\}$ is increasing and, since it is also bounded, convergent. By comparing these results with those of Section 3.2, it is obvious that $\lambda_1^{(m)}(s) \to \lambda_1(s)$. This convergence is very fast, as shown in Figure 3 for $\rho = 1, 10, 20$.

The results of this section justify using the infinite leaf model of Section 2.2. Although the assumption is biologically unrealistic, from Figure 3 we conclude that limiting leaf size (such that the maximum age is, say, between 10 and 20 days, or the spot sizes are only 4 to 8 cm) produces essentially similar results for the speed of invasion.

Two idealizations have been made to arrive at a predicted speed: neglecting nonlinear terms and approximating the sequence of increasing, finite matrices with an asymptotic infinite matrix. Two questions, therefore, remain unanswered:

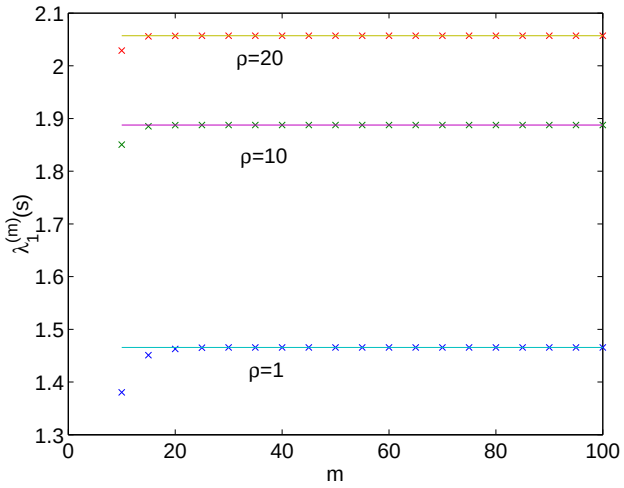

Figure 3: Convergence of $\lambda_1^{(m)}(s)$ (denoted by $\times$) to $\lambda_1(s)$ (solid) for ρ=1, 10 and 20. Here m is both the number of days (generations) since simulation inception and the order of the matrix. Convergence is rapid in all cases, so that by the twentieth generation of an infestation the finite and infinite values are the same for all practical purposes.

- How much is the invasion speed, v_{nl}, obtained from the realistic model (2) overestimated by the invasion speed, v_{l}, obtained from the linearized model (6)?
- How well does the theoretical bound for invasion speed v^* approximate the speed of the linearized model v_{l}, given that the infinite matrix is an approximation to the iteration of operators of finite, but growing, dimension?

These questions are addressed numerically below.

4 Numerical Tests

In numerical simulations we considered two types of dispersal kernels in (4): the Gaussian kernel,

$$K(x) = \frac{1}{\sigma\sqrt{2\pi}}\, e^{-\frac{x^2}{2\,\sigma^2}}, \tag{24}$$

and the Laplace kernel

$$K(x) = \frac{1}{2\,\sigma}\, e^{-\frac{|x|}{\sigma}}, \tag{25}$$

where σ is the mean distance traveled by spores in meters (nominally set to 1 meter). These two kernels are among the most commonly used for dispersal studies. The Gaussian form describes a process of random dispersion in the horizontal direction as spores fall from a given height to

the ground; the Laplace kernel describes the net results of a random horizontal diffusion in time coupled with a constant rate of precipitation of spores to the ground. It is important to check the sensitivity of the results to dispersal; the amount of infectious material increases without bound, and so it is possible that the 'heavy tail' of the Laplace distribution could lead to continually accelerating fronts and divergence between predictions and observations. Convolution and dispersal were implemented using Fast Fourier Transforms and the property that the transform of the convolution is the product of the transforms. In all simulations 4096 grid points were used; the size of the spatial domain was $180 \times v^*$ meters, where v^* is the maximum predicted velocity. Given initial conditions starting in the center of the domain, this gave enough space so that in 60 'days' of simulation a developing front had 1.5 times as much room to propagate as the maximum speed linear prediction. Boundary conditions were taken to be periodic.

Each simulation was performed in the non-linear case using (2), where P_{un} from (3) was recomputed in each step (each day) using formula (1), and in the linearized case using (6). The behavior of P_{un} and shape of typical fronts for parameters as in Table 1 and both Laplace and Gaussian kernels is depicted in Figure 4, for both linear and nonlinear growth rates. In both cases, P_{un} was used to diagnose and depict the location of the front; that is, to determine the location of the wave of invasion each 'day' we would calculate P_{un} (even if it was not used in the dynamics, as in the linear simulations) and determine the current extent of the invasion by determining which grid cell contained that point where $P_{\text{un}} = \frac{1}{2}$. From the obtained results we then deduced the speeds of invasion (v_{nl} and v_{l}, respectively) in both non-linear and linear settings by calculating the distances propagated over 10 days at the end of the simulation.

For each simulation we also computed the upper bound of the invasion speed v^* from (10) as follows: we multiplied the composite constant R from (5) and the moment generating function $M(s)$ from (8) to obtain ρ from (18). This ρ was then inserted into (23) to obtain $\lambda_1(s)$. Finally, $\lambda_1(s)$ was inserted into (10), and the minimum over s was computed, giving v^*. The speed of invasion v^* should match the speed obtained by the simulation in the linearized case. According to (8), the moment generating function is given by

$$M(s) = e^{\frac{\sigma^2 s^2}{2}}$$

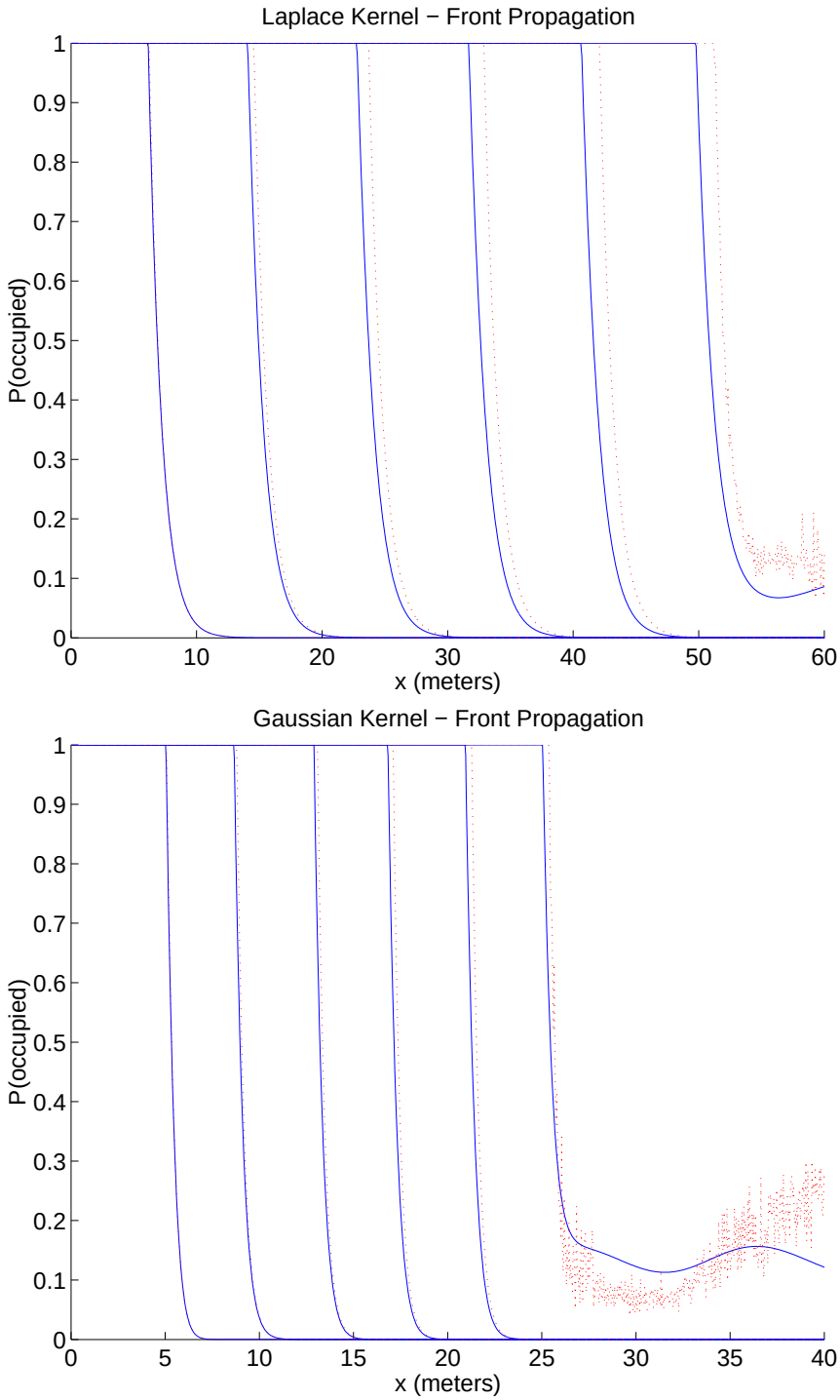

Figure 4: Evolution of the front from initial conditions $N_1^0 = 10^4, |x| < 3, N_*^0 = 0$ otherwise, in the case of the Laplace kernel (top) and Gauss kernel (bottom), with nominal parameters as given in Table 1. The fraction of resource *occupied*, $1 - P_{\text{un}}$, is plotted here. Time slices are ten days apart, with the evolution of the nonlinear front given by solid lines and the linear front given by dotted lines. Notice that during the last time slice small round-off errors have grown in advance of the front; these eventually grow and dominate the solution. The nonlinear solution looks much smoother at this point because calculation of P_{un} involves summing over age classes, smoothing the instability.

for the Gaussian kernel (24), and by

$$M(s) = \frac{1}{1 - \sigma^2 s^2},$$

for the Laplace kernel (25).

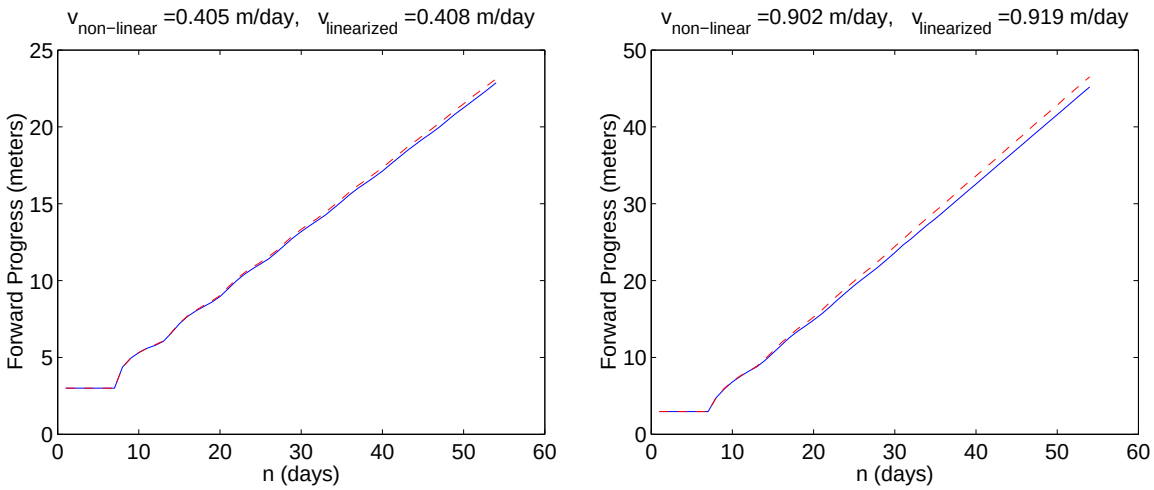

Gaussian kernel Laplace kernel

Figure 5: Progress of an invasion with mean spore dispersal distances of 1 meter using Gaussian (left) and Laplace (right) kernels. Parameters are set to nominal values described in Table 1. Invasions were allowed to progress linearly (unoccupied resource fraction, P_{un}, set always to 1, dashed lines) and nonlinearly (solid lines). The predicted speeds are $v^* = 0.415$ meters/day for the Gaussian kernel and $v^* = 0.936$ meters/day for the Laplace kernel, which is a small overestimate of the linear propagation speeds and a larger overestimate of the nonlinear speeds.

Figure 5 shows an example of simulation with nominal values of parameters from Table 1. For these values, the composite constant R from (5) and (17) is equal to $R = 10.0531$. The simulation was run with Gaussian and Laplace kernel, respectively, with $\sigma = 1$ meter in both cases. Solid curves show the progress of infection in the non-linear cases, and dashed curves show the progress in the linearized cases with $P_{\text{un}} = 1$ in (3). For this example the theoretical speeds are $v^* = 0.415$ meters/day for the Gaussian kernel and $v^* = 0.936$ meters/day for the Laplace kernel. We see that, for both kernels, the speeds obtained by linearization, v_{l}, overestimate the speeds of the nonlinear model, v_{nl}, and the theoretical speeds v^* slightly overestimate v_{l}. This is quite interesting, as the dynamic perspective on front propagation suggests that v^* should be the asymptotic speed for both linear and nonlinear fronts, and simulation results with fixed-size Leslie matrices indicate rapid convergence to the predicted minimal wave speed (see, for example, Neubert and Caswell [19]).

To more completely investigate the comparative behavior of v_{nl} and v_{l} versus v^*, we performed a series of simulations with different values of parameters from Table 1 in a randomized factorial design. The first three parameters (SI, LP and IP) were kept at nominal values, while the remaining five parameters were chosen as follows:

$$\begin{aligned} P_{\text{inf}} &\in \{0.0075, 0.01, 0.0125\}, \\ P_{\text{int}} &\in \{0.075, 0.1, 0.125\}, \\ \Delta r &\in \{1 \times 10^{-3}, 2 \times 10^{-3}, 3 \times 10^{-3}, 4 \times 10^{-3}\}, \\ LAI &\in \{3, 5, 7\}, \\ \sigma &\in \{0.5, 1, 1.5, 2\}. \end{aligned}$$

This gives 432 simulations for each kernel. The composite constant R attained values in the interval $R \in [0.3534, 15.7080]$, and the theoretical bound for invasion speed v^* attained values $v^* \in [0.1198, 0.8755]$ for the Gaussian kernel and $v^* \in [0.2376, 2.0106]$ for the Laplace kernel. Simulation results are summarized in Figure 6.

The disparity between observation and prediction depicted in Figure 6 reflects what appears to be a consistent overprediction of observed linear and nonlinear speeds, with the degree of overprediction being approximately twice as large for nonlinear speeds as for linear speeds. The explanation lies in three interrelated effects. Firstly, the net daily per-capita growth rate for fungal lesions was never less than 1.5 in our simulations, and often as large as 10, reflecting the extremely invasive nature of late blight. As a consequence, simulations were difficult to run for long periods of time; at some point small round-off errors in the neighborhood of zero grew geometrically. In practice we were unable to maintain simulations much beyond 50 iterations, and running longer simulations to allow for greater convergence was impossible both because of the extreme instability of the zero population state as well as the size of the transition matrices (which are as large as the number of days) at each spatial location.

Confounded with this are *two* convergence effects, each contributing to overprediction. In the first place there is the convergence to the stable traveling population distribution, which is described by the first neglected terms in the power method. Thus, when considering the evolution of a front from compact initial data, the asymptotic problem should read

$$e^{ns^*v^*}\ \vec{w} = \mathbf{H}^n(s^*)\ \vec{w} \quad = \quad a_1(s^*)\lambda_1^n\vec{e}_1(s^*) + a_2(s^*)\lambda_2^n\vec{e}_2(s^*) + \cdots$$

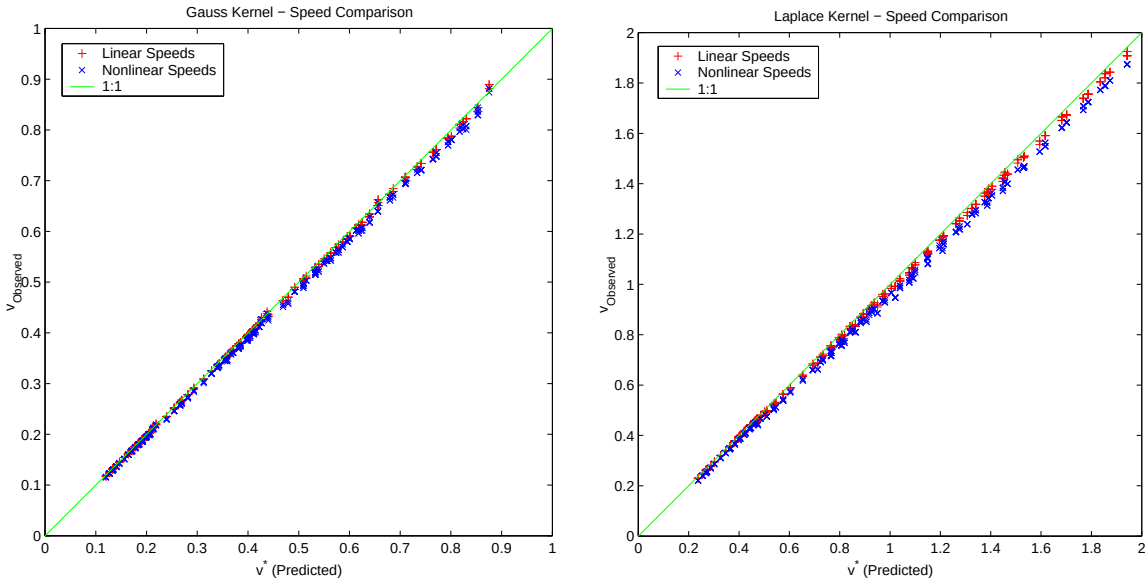

Figure 6: Comparison of predicted and observed speeds for waves of invasion with and without density dependent growth restrictions for both Laplace and Gaussian dispersal kernels. Parameters are chosen in a random factorial design described in the text, with variation centered on the nominal values described in Table 1. Observed linear and nonlinear speeds are marked with '$+$' and '$\times$' respectively. The solid line is the line $v_{\text{observed}} = v_{\text{predicted}}$, indicating perfect agreement. Results indicate a consistent overprediction of observation by prediction, with a greater degree of error for nonlinear as compared to linear propagation.

$$= \lambda_1^n \left[a_1(s^*)\vec{e}_1(s^*) + a_2(s^*)\frac{\lambda_2^n}{\lambda_1^n}\vec{e}_2(s^*) + \cdots \right].$$

Here $\vec{e}_1(s^*)$ can be interpreted as the asymptotic stable population distribution selected by the wave of invasion, while $\vec{e}_2(s^*)$ is the age structure of the 'ringing' which occurs as population distributions converge to the stable distribution along a front. The ratio of the largest and second-largest magnitude eigenvalues is the rate of convergence. This is asymptotically negligible, but for finite simulations we may expect an error proportional to

$$E_{\text{Power}} \sim |\vec{e}_1 \cdot \vec{e}_2| \frac{|\lambda_2|^n}{|\lambda_1|^n}. \tag{26}$$

The second convergence effect is the natural acceleration of the front to the asymptotic front speed described by (16). Predicted by steepest descents, this is the convergence of the spatial shape of the front to its asymptotic exponential shape, a translate of e^{-s^*x}. The speed convergence error is (from 16)

$$E_{\text{Speed}} \sim \frac{\ln(n)}{2nk^*}. \tag{27}$$

While E_{Speed} tends to zero as n tends to infinity, the convergence is slow, and again the error can not be neglected for short simulations.

To investigate how these errors relate to observed errors in our simulation we ran each of the factorially crossed parameter studies for as long as possible, diagnosing the onset of overwhelming instability by the inevitable sudden jump in the rate of progress of the front. In each simulation the day at which the simulation 'broke' was diagnosed by and recorded as $nday$. During each simulation the forward progress (x_{fp}) of the front was diagnosed as described above. Observed speeds were then

$$v_{\text{observed}} = \frac{x_{fp}(nday - 5) - x_{fp}(nday - 15)}{10}.$$

The largest two eigenvalues of the finite transition matrix, $\lambda_1^m(s^*)$ and $\lambda_2^m(s^*)$, were calculated, with m evaluated at the center of the speed calculation interval, $m = nday - 10$. This information determines the size of the two error components, E_{Power} and E_{Speed}. These errors are compared to the observed relative speed error,

$$\frac{v^* - v_{\text{observed}}}{v^*},$$

in Figure 7. Errors for the Laplace kernel were similar, but of smaller size. In each case, $E_{\text{Power}} + E_{\text{Speed}}$ is a close upper bound on the size of observed errors.

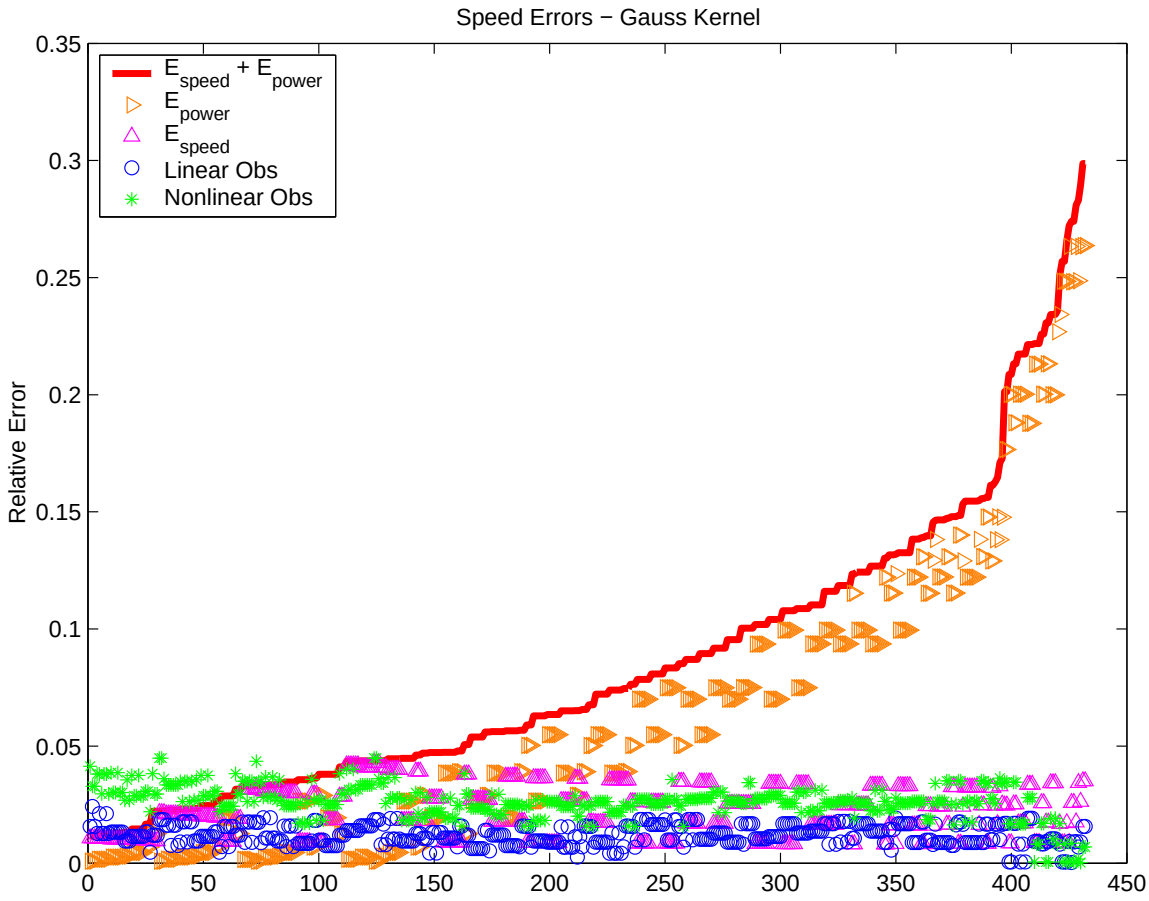

Figure 7: Raw comparison of observed relative speed errors in the nonlinear (‘*’) and linear (‘$\circ$’) cases for the Gaussian kernel, with randomized choices of parametric data, centered on the nominal values in Table 1. The asymptotic error size due to age structure convergence, E_{Power}, is plotted as ‘$\triangleright$’, while asymptotic error size due to speed convergence, E_{Speed}, appears as ‘$\triangle$’. The total error size, $E_{\text{Speed}} + E_{\text{Power}}$ is the solid line; results were sorted in terms of increasing total error. The horizontal axis is the identifying index of the simulation and has no units. Given that the actual error relates by an order one factor to the error sizes depicted here, both the linear and nonlinear front speeds are well within acceptable error bounds.

5 Conclusion

We have shown in this paper how to extend the methodology of Neubert and Caswell [19], incorporating age structure and dispersal into integrodifference population models, to infinite dimensional cases of lesion-based diseases. Not only is the infinite dimensional version easier to analyze than the finite version, but the results are very close to wave speed observed in the finite case. Even in the extremely invasive late potato blight the agreement between analytic results and simulations are well within expected error tolerances. The minimum wave speed, given by the infinite dimensional version of (10), is an upper bound for rates of invasion propagation and seems to be the asymptotic speed selected for waves of invasion, as suggested by the dynamic interpretations of Dee and Langer [3] and Powell et al. [23, 24]. In fact, results in this paper suggest that the dynamic interpretation has the additional virtue of accurately describing convergence rates to the asymptotic wave speed.

We have also described a modeling approach for lesion-based foliar diseases, which may find potential application in any sort of invasion process where growing patches are the basic unit of infection. Examples include cheat grass in the American West [29], pathogenic fungi of the genus *Botrytis* (which cause 'fire disease' in flower crops and infect field and greenhouse vegetables, small fruits, ornamental plants, flower bulbs and forest tree seedlings world wide [13]), and insects such as the Southern Pine Beetle (which create 'spot' infections in patches of pine forest [25]) or gypsy moth, which seems to invade by via spots [27]. Even reproduction and spread of forests may fit; trees could be regarded as an assembly of branches whose reproduction is linearly increasing in time as the tree adds branches. Thus the individual tree would take the role of the 'lesion' and the approach would remain fundamentally the same. By no means is this the first attempt at modeling spread of late blight and fungal pathogens (see, for example van den Bosch et al. [37] and Pielaat and van den Bosch [22]), nor (more generally) age structured spread in general (see Hengeveld [10] and Shigesada and Kawasaki [29] for reviews). But it *is* the first attempt that we know of to put the concept of an ever-growing infection structure on the relatively firm and simple ground of a Leslie matrix formulation.

The drawback in the modeling approach used here is the difficulty in accounting for two factors: finite leaf size and coalescence of lesions. The first factor is not too difficult to imagine incorporating, though possibly tedious. At the coarsest level, when lesions grow to the average

size of a leaf they can grow no more, which amounts to truncating the nonlinear Leslie matrix at an age class of lesions corresponding to the area of the largest leaves. At a slightly less coarse scale, in plants with a size distribution of leaves, one would need to estimate the probability of a lesion using up all available area by the probability that it had landed on a leaf of its current size. This would give a transition probability of smaller than one for lesions larger than a certain size, which would drop to zero for lesions at the largest leaf size. Finally, when lesions grow on finite substrates they will eventually encounter boundaries, and while they may continue to grow the new growth area will no longer be annular. Consequently some estimate is needed of the probability of observing annular growth of area ΔA_t, which would then alter the rate at which new lesions are formed. In all of these cases, incorporation of realistic leaf sizes would ruin the special matrix structure which allowed for analytic calculation of the largest magnitude eigenvalue, though the theory predicting the existence of a single, largest eigenvalue would remain in place.

The second factor, coalescence of lesions on a leaf, would be somewhat more difficult to address. Shigesada and Kawasaki [29] outline a procedure for approximating the rate at which patches of an invasive species run into one another. The basic idea is to model the process as a summation, so that when two circular patches encounter one another they are approximated as a new patch of size equal to the sum of the previous patches. Knowing the distribution of distances at which patches are established and their radial growth rates, one can predict the mean time until patches encounter one another. In our age-structure framework this would manifest as a new kind of transition probability: among all age classes would be a class of transitions which would allow a lesion of a given size to sum with a lesion of any other size and create a new lesion in a size class equal to the sum of the two. The resulting transition matrix would be lower triangular (except for the top row, representing the production of new lesions), and have nonzero entries up to the point where maximum dispersal distance and radial growth no longer allow for two lesions to coalesce (i.e. when the size of the lesion is greater than its capacity for dispersal). At this stage new theoretical difficulties are bound to be encountered; the infinite dimensional version of the size class/dispersal formalism was relatively easy to describe in the current case due to the simple form of the Leslie matrix involved.

Both of these factors, however, clearly *reduce* the growth rate of the lesion population and would slow down the wave of invasion. Consequently we may expect the v^* calculated above to

remain an upper bound for the speed of invasions. It is then particularly useful since part of the calculation can be performed analytically, given the simple algebraic form of the largest eigenvalue for the infinite dimensional system.

Acknowledgments

Groundwork for this manuscript was laid during a sabbatical visit by Dr. Powell to Wageningen University in the Netherlands, funded in part by NSF grant INT-9813421 and by the Wageningen University Research School for Production Ecology and Resource Conservation. Dr. van der Werf gratefully acknowledges the Dutch Technology Foundation STW and the Programme on Biological Resource Management for Sustainable Agricultural Systems of OECD for providing resources to make critical visits to Utah State University as well as a grant from the OECD. Further support was provided by Strategic Expertise Development Project 620-33001-76 of Plant Research International, Wageningen. We acknowledge helpful conversations with Dr. Geert Kessel, who read an earlier version of this manuscript and provided biological commentary. This manuscript was written during the sabbatical visit by Dr. Slapničar to the Department of Mathematics and Statistics at the Utah State University, Logan, Utah, and Dr. Slapničar acknowledges grant 0023002 of the Croatian Ministry of Science and Technology.

References

[1] CIP in 1995. The International Potato Center Annual Report. Lima, Peru.

[2] Caswell, H., R. Lensink & M.G. Neubert, 2003. Demography and dispersal: life table response experiments for invasion speed. Ecology 84, 1968-1978.

[3] Dee, G. and J.S. Langer 1983. Propagating pattern selection. *Physical Review Letters* **50**: 383–386.

[4] Diekmann, O. & J.A.P. heesterbeek, 2000. Mathematical epidemiology of infectious diseases. Wiley, Chichester, 303 pp.

[5] Duncan, J.M. 1999. *Phytophthora*- an abiding threat to our crops. *Microbiology Today* **26**: 114 - 116.

[6] Erwin, D. C. and Ribeiro, O. K. 1996. *Phytophthora* diseases worldwide, American Phytopathological Society (APS Press), St. Paul, Minnesota, USA, 562 pages.

[7] Fisher, R. 1937. The wave of advance of an advantageous gene. Annual Eugenics **7**:355–69.

[8] Flier, W.G. and Turkensteen, L.J. 1999. Foliar aggressiveness of *Phytophthora infestans* in three potato-growing regions in the Netherlands. *European Journal of Plant Pathology* **105**: 381 - 388.

[9] Halberg, C.J.A. 1955. Spectral Theory of Linked Operators in the Spaces l_p, Ph.D. Thesis, University of California, Los Angeles, 69 pages.

[10] Hengeveld, R. 1994. Small-step invasion research. *Trends in Ecology and Evolution* **9**: 339–342.

[11] Hooker, W.J. 1981. Compendium of potato diseases. American Phytopathological Society, ST. Paul, MN.

[12] de Jong, M.D., G.W. Bourdôt, J. Powell and J. Goudriaan. 2002. A model of the escape of *Sclerotinia sclerotiorum* ascospores from pasture. To appear, *Ecological Modelling*.

[13] Kessel, G.J.T., B.H. de Haas, C.H. Lombaers-van der Plas, J.E. van den Ende, M.G. Pennock-Vos, W. van der Werf and J. Khl, 2001. Comparative analysis of the role of substrate specificity in biological control of Botrytis elliptica in lily and B. cinerea in cyclamen with Ulocladium atrum. European Journal of Plant Pathology 107, 273-284.

[14] Kolmogorov, A., I. Petrovsky, and N. Piscounoiv. 1937. Etude de l'équation de la diffusion avec croissance de la quantité de la matière et son application a un problème biologique. *Bulletin of University of Moscow, Series A* **1**:1–25.

[15] Kot, M., M.A. Lewis, and P. van den Driessche. 1996. Dispersal data and the spread of invading organisms. *Ecology* **77**:2027–2042.

[16] Kot, M. 1992. Discrete-time travelling waves: ecological examples. *Journal of Mathematical Biology* **30**: 413–436.

[17] Lamour, A., 2000. Quantification of fungal growth models: models, experiments, and observations. PhD Thesis, Wageningen University, 132 pp.

[18] Lancaster, P. 1969. Theory of Matrices, Academic Press, New York.

[19] Neubert, M.G., and H. Caswell 2000. Demography and dispersal: Calculation and sensitivity analysis of invasion speed for structured populations. *Ecology* **81**:1613–1628.

[20] Lewis, M.A, B. Li and H.F. Weinberger 2002. Spreading speed and linear determinacy for two-species competition models. J. Math. Biol. 45 (2002), no. 3, 219–233.

[21] Neubert, M.G., M. Kot, and M.A. Lewis. 1995. Dispersal and pattern formation in a discrete-time predator-prey model. *Theoretical Population Biology* **48**:7–43.

[22] Pielaat, A. and F. van den Bosch. 1998. A model for dispersal of plant pathogens by rain-splash. *IMA Journal of Mathematics Applied in Medicine and Biology* **15**: 117-134.

[23] Powell, J. 1997. Conditional stability of front solutions, *J. Math. Biol* **35**: 729–47.

[24] Powell, J., A.C. Newell and C.K.R.T. Jones 1991. Competition between generic and non-generic fronts in envelope equations, *Phys. Rev. A* **44**, 3636–3652.

[25] Meeker, J. R., W. N. Dixon, and J. L. Foltz. 1995. The southern pine beetle, Dendroctonus frontalis Zimmermann (Coleoptera: Scolytidae). Florida Dept Agric Cons Serv, Div Plant Industry Entomology circular No. 369. 4 p.

[26] Paysour, R. E. and Fry, W. E. 1983. Interplot Interference: A model for planning field experiments with aerially disseminated pathogens. Phytopathology 73(7): 1014-1020.

[27] Sharov, A. A., and A. M. Liebhold. 1998. Model of slowing the spread of gypsy moth (Lepidoptera: Lymantriidae) with a barrier zone. *Ecol. Appl.* **8**: 1170-1179.

[28] Segarra, J., M.J. Jeger & F. van den Bosch, 2001. Epidemic dynamics and patterns of plant diseases. Phytopathology 91, 1001-1010.

[29] Shigesada, N., and K. Kawasaki. 1997. Biological Invasions: Theory and Practice. Oxford University Press, Oxford, 205 pages.

[30] Skellam, J.G. 1951. Random dispersal in theoretical populations. Biometrika **38**:196–218.

[31] Taylor, A.E. and Lay, D.C. 1980. Introduction to Functional Analysis, 2nd edition, Wiley, New York, 465 pages.

[32] Turkensteen, L.J. 2002. Personal communication.

[33] van den Bosch, F., H.D. Frinking, J.A.J. Metz & J.C. Zadoks, 1988a. Focus expansion in plant disease. III. Two experimental examples. Phytopathology, 78, 919-925.

[34] van den Bosch, F., J.C. Zadoks & J.A.J. Metz, 1988b. Focus expansion in plant disease. III. Realistic parameter-sparse models. Phytopathology 78, 59-64.

[35] van den Bosch, F., J.C. Zadoks & J.A.J. Metz, 1988c. Focus expansion in plant disease. I. The constant rate of focus expansion. Phytopathology, 78, 54-58.

[36] van den Bosch, F., M.A. Verhaar, A.A.M. Buiel, W. Hoogkamer & J.C. Zadoks, 1990. Focus expansion in plant disease. IV. Expansion rates in mixtures of resistant and susceptible hosts. Phytopathology 80, 598-602.

[37] van den Bosch, F., R. Hengeveld and J.A.J. Metz. 1994. Continental expansion of plant disease: a survey of some recent results. Pages 274-281 *in* J. Grasman and G. van Straten, editors. Predictability and nonlinear modelling in natural sciences and economics. Kluwer Academic, Dordrecht, the Netherlands.

[38] Weinberger, H.F. 1978. Asymptotic behavior of a model of population genetics. Pages 47-96 *in* J. Chadam, editor. Nonlinear partial differential equations and applications. *Lecture Notes in Mathematics* **684**.

[39] Weinberger, H.F. 1982. Long-time behavior of a class of biological models. *SIAM J. Math. Anal.* **13**: 353–396.

[40] Weinberger, H.F., M.A. Lewis and B. Li 2002. Analysis of linear determinacy for spread in cooperative models. J. Math. Biol. 45, no. 3, 183–218.

[41] Zadoks, J.C. and Schein, R.D. 1979. Epidemiology and Plant Disease Management. Oxford University Press, Oxford, UK. 427 pages.